Corrosion Science xxx (2011) xxx–xxx

Contents lists available at SciVerse ScienceDirect

Corrosion Science

journal homepage: www.elsevier.com/locate/corsci

Molecular dynamic and quantum chemical calculations for phthalazine derivatives as corrosion inhibitors of mild steel in 1 M HCl

Ahmed Y. Musa [a,b,*], Ramzi T.T. Jalgham [b], Abu Bakar Mohamad [b]

[a] Department of Chemistry, The University of Western Ontario, 1151 Richmond Street, London, Ontario, Canada N6A 5B7
[b] Department of Chemical and Process Engineering, Universiti Kebangsaan Malaysia, Bangi, 43600 Selangor, Malaysia

ARTICLE INFO

Article history:
Received 29 July 2011
Accepted 7 December 2011
Available online xxxx

Keywords:
A. Mild steel
B. Modeling studies
C. Acid inhibition

ABSTRACT

The abilities of phthalazine derivatives, including phthalazine (PT), phthalazone (PTO) and phthalhydrazide (PTD), to inhibit the corrosion of mild steel in 1 M HCl at 30 °C were studied using electrochemical impedance spectroscopy (EIS) and potentiodynamic polarization measurements. Theoretical calculations were performed to investigate the electronic structures of the PT derivatives. Our results showed that the inhibition efficiencies of these derivatives improved with increases in concentration. The data also showed that PTD < PT < PTO in terms of the inhibiting efficiency. Theoretical calculations also revealed that PTO is expected to be the best inhibitor among the studied phthalazine derivatives.

1. Introduction

The corrosion of metals, including mild steel, is a serious problem in many industries, especially during processes such as the pickling of steel, acid washing and etching [1,2]. Corrosion inhibitors are chemical compounds that in small quantities can retard the degradation of metals in hostile environments. Because these inhibitors represent an economic and effective technique to prevent metal and alloys from being corrupted, inhibitors are widely used in chemical cleaning solutions, industrial water and petrochemical engineering production processes, applied to the atmosphere and environment and are becoming an indispensable protection measure during industrial production [3]. These inhibitors are believed to work by influencing the kinetics of the electrochemical reactions that constitute the corrosion process, thereby modifying the metal dissolution in acids. The existing data show that most organic inhibitors act by adsorption onto the metal surface [4]. Generally, organic inhibitor molecules might physically or chemically adsorb onto a corroding metal.

Theoretical chemistry, including quantum chemical calculations, has proved to be a very powerful tool for studying the mechanism of corrosion inhibition [5]. Because strong correlations have been found between the corrosion inhibition efficiencies of most compounds with several semi-empirical parameters, the quantum chemical principle is a useful tool to predict the inhibition potentials of structurally related organic compounds [6–10]. A better understanding of how inhibitor molecules behave on a metal surface could greatly enhance our ability to control the essential interfacial properties of these systems in a wide variety of corrosion problems. As such, the adsorption of inhibitor molecules on surfaces has recently become the subject of intensive investigation in the field of corrosion research [11–22].

The objectives of this work were to study the inhibition performance of phthalazine derivatives, namely phthalazine (PT), phthalazone (PTO) and phthalhydrazide (PTD) (Fig. 1), using electrochemical impedance spectroscopy (EIS) and potentiodynamic polarization measurements. Properties of the molecular structure of these phthalazine derivatives were calculated using AM1, PM3 and MNDO semi-empirical equations implemented with Restricted Hartree–Fock (RHF). Monte Carlo molecular simulations were performed using an adsorption locator module to obtain adsorption energies of the phthalazine derivatives on the Fe_2O_3 surface.

2. Materials and methods

Mild steel specimens with an exposed area of 4.5 cm^2 were obtained from the Metal Samples Company (PA, USA) and were used as the working electrodes throughout this study. The compositions (wt.%) of mild steel in the electrodes are listed in Table 1. The studied inhibitors, PT, PTO and PTD, were supplied by Sigma–Aldrich Co. and were used without any further purification. The inhibitor concentrations ranged from 0.25 to 2 mM. The 1 M HCl solution was prepared by dilution of analytical grade 37% HCl with distilled water. Measurements were performed in a non-aerated and unstirred 1 M HCl acid solution at 30 °C (±1 °C). The temperature

* Corresponding author at: Department of Chemistry, The University of Western Ontario, 1151 Richmond Street, London, Ontario, Canada N6A 5B7. Tel.: +1 519 661 2111x86312; fax: +1 519 661 3022.
E-mail addresses: AMUSA6@UWO.CA, ahmed.musa@ymail.com (A.Y. Musa).

0010-938X/$ - see front matter © 2011 Elsevier Ltd. All rights reserved.
doi:10.1016/j.corsci.2011.12.005

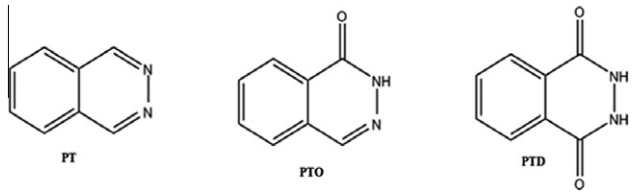

Fig. 1. Chemical structure of the investigated Phthalazine derivatives inhibitor.

was controlled using a thermostat [23]. The specimens were cleaned according to ASTM standard procedure G1-03 [24].

A 200 mL, Gamry water-jacketed glass cell was used in these experiments. The cell contained the three classic electrodes, namely the working, counter and reference electrodes, which were comprised of mild steel, a graphite bar and a saturated calomel electrode (SCE), respectively [25,26]. Measurements were performed using a Ref 600 model Gamry Instrument Potentiostat/Galvanostat/ZRA. The DC105 and EIS300 software by Gamry were used for electrochemical impedance spectroscopy (EIS) and potentiodynamic scans, respectively. The potentiodynamic current–potential curves were taken from −0.2 to +0.2 V_{SCE} at a scan rate of 0.5 mV s^{-1}. Impedance measurements were performed using AC signals with a 10 mV peak-to-peak amplitude at the open circuit potential in the frequency range of 10 kHz–0.1 Hz. All impedance data were fitted to appropriate equivalent circuits (ECs) using Gamry Echem. Analyst software. Electrochemical measurements were initiated approximately 30 min after the working electrode was immersed in solution to stabilize the steady-state potential [25,27].

3. Theoretical calculations

Theoretical studies were performed to examine the electrostatic structures of the PT derivatives in order to compare the theoretical and experimental results. Our goal was to investigate the relationships between the PT derivatives' inhibition abilities and their quantum chemical parameters. Molecular simulation studies were performed using the Materials Studio software (Version 5.5) from Accelrys Inc. This software is a high-quality quantum mechanics computer program that is available from Accelrys (San Diego, CA) [28]. Our study employed three modules. As described on the Accelrys website, the VAMP module "is a semi-empirical molecular orbital package for molecular organic and inorganic systems." The Forcite module "is an advanced classical molecular mechanics tool that allows fast energy calculations and reliable geometry optimization of molecules and periodic systems." Finally, the Adsorption locator module "identifies possible adsorption configurations by carrying out Monte Carlo searches of the configurational space of the metal-adsorbate system as the temperature is slowly decreased (simulated annealing)." In this study, the molecules were sketched, the hydrogens were adjusted and the molecules were cleaned using sketch tools available in the Materials Visualizer.

Table 1
Composition of the mild steel electrode.

Element	Content (wt.%)
Fe	99.21
C	0.21
Si	0.38
P	0.09
S	0.05
Mn	0.05
Al	0.01

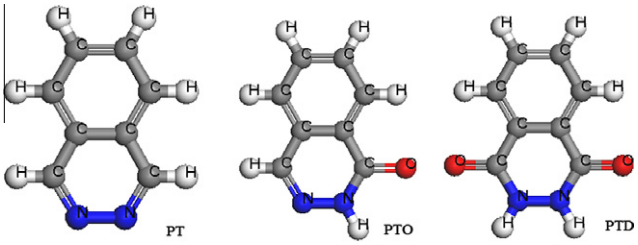

Fig. 2. Sketches ofmolecules of the PT derivatives.

The sketched molecules are shown in Fig. 2. All quantum calculations were performed with complete geometry optimization using the VAMP module and performed at the restricted Hartree–Fock (RHF) level using AM1, PM3 and MNDO semi-empirical methods in the Materials Studio software [29,30]. The molecules that are shown in Fig. 2 were optimized (i.e., energy minimizing) in the Monte Carlo simulations using the Forcite module and the Condensed-Phase Optimized Molecular Potentials for Atomistic Simulation Studies (COMPASS) force field, as shown in Fig 3. COMPASS is the first *ab initio* force field that has been parameterized and validated using condensed-phase properties in addition to various *ab initio* and empirical data for molecules in isolation. Consequently, this force field enables accurate and simultaneous prediction of structural, conformational, vibrational and thermophysical properties for a broad range of molecules in isolation and in condensed phases and under a wide range of temperatures and pressures. The unit cell structures of metal oxides with the associated experimental lattice parameters were available from Materials Studio. Using the surface builder module of Materials Studio, metal oxide surfaces were prepared by employing the desired cleavage planes hkl (1 1 0). This provided the fractional depth of the surface, which should be larger than the non-bonded cut-off distance of 9.5 Å [31].

The choice of cut-off is always a trade-off between the accuracy of the results and the time required for the calculation. Using a thickness of 4.3 Å, which produces a depth of approximately 10.83 Å for a Fe_2O_3 surface, a depth is obtained which is sufficient for the inhibiter molecules to only be involved in non-bonded interactions with the Fe_2O_3 atoms on the surface, and this calculation can be completed in a reasonable time. The surface must be large enough to accommodate the inhibiter molecules; therefore, a distance monitor was used to calculate the length of the optimized molecules, yielding 6.065, 7.033 and 7.066 Å for PT, PTO and PTD, respectively, as shown in Fig. 3. We used super cell package to triple U × V (3 × 3) in order to expose a more realistic surface area for docking the inhibitor molecules. This step produced a surface with parameters of 16.25 and 18.5 Å, which is enough to accommodate the inhibitor molecules. It is important that the size of the vacuum is great enough such that the non-bonded calculation for the adsorbate does not interact with the periodic image of the bottom layer of atoms in the surface; thus, a vacuum slab with thickness 40 Å was built using Crystal Builder.

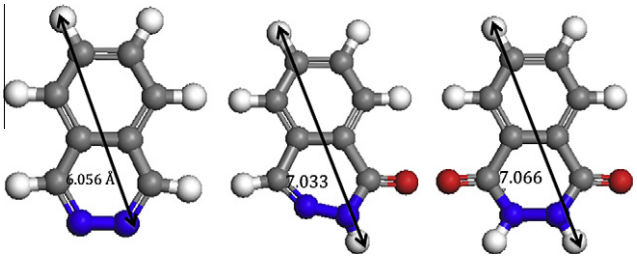

Fig. 3. Optimized structures of the PT derivatives using Forcite.

Please cite this article in press as: A.Y. Musa et al., Molecular dynamic and quantum chemical calculations for phthalazine derivatives as corrosion inhibitors of mild steel in 1 M HCl, Corros. Sci. (2011), doi:10.1016/j.corsci.2011.12.005

The molecular dynamic simulation considers a metal loaded with an adsorbate. A low-energy adsorption site is identified by performing a Monte Carlo search, and this process is repeated to identify further local energy minima. During the course of the simulation, adsorbate molecule are randomly rotated and translated around the metal. The configuration that results from each of these steps is accepted or rejected according to the selection rules of the Metropolis Monte Carlo method. The force field used was COMPASS. The adsorption surface region defined by the atom set and top layer was chosen as a target with a maximum distance of 15 Å from the adsorbate to the selected target [32].

4. Results and discussion

4.1. Electrochemical impedance spectroscopy (EIS) measurements

The Nyquist plots obtained for mild steel in 1 M HCl in the absence and presence of various concentrations of the PT, PTO and PTD molecules are shown in Figs. 4–6, respectively. These plots were characterized by one depressed semi-circular capacitive loop at high frequency, which is then followed by one small inductive loop at low frequency. The impedance spectra present an almost perfect semicircle, the center of which lies under the real axis. Such phenomena often refer to the frequency dispersion of interfacial impedance, which has been attributed to the roughness, or inhomogeneity, of the solid surfaces and adsorption of inhibitors [8]. Therefore, a constant phase element (CPE) is used instead of a capacitive element to obtain a more accurate fit of our experimental data sets, using generally more complicated equivalent circuits. The CPE impedance is given by [33]:

$$Z_{CPE} = A^{-1}(i\omega)^{-n} \quad (1)$$

In this equation, A is the CPE constant, ω is the angular frequency (in rad s^{-1}), $i^2 = -1$ (the imaginary number) and n is a CPE exponent that can be used as a gauge of the heterogeneity, or roughness, of the surface. The equivalent circuit model employed for this system is shown in Fig. 7 and consists of an uncompensated solution resistance R_u in series to the parallel resistor of charge transfer (R_{ct}) and constant phase element (CPE) connected to its exponent. It can be observed that in Figs. 4–6, the total impedance in the recorded Nyquist plots increases with an increase of the inhibitor concentration. These plots are fitted to a circuit model using Gamry Analyst software, and the fitted values are listed in Table 2. Because the impedance of the inhibited mild steel

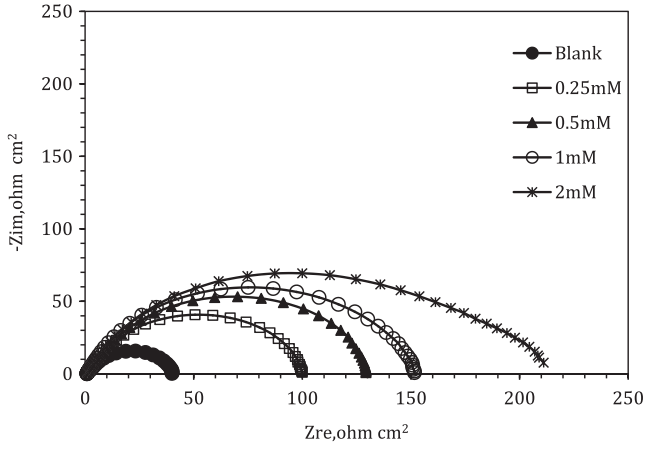

Fig. 4. Nyquist plots for mild steel in 1 M HCl at 30 °C in the absence and presence of various concentrations of PT.

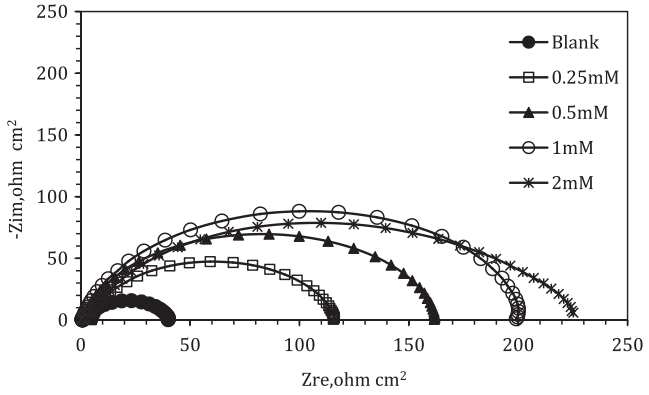

Fig. 5. Nyquist plots for mild steel in 1 M HCl at 30 °C the in absence and presence of various concentrations of PTO.

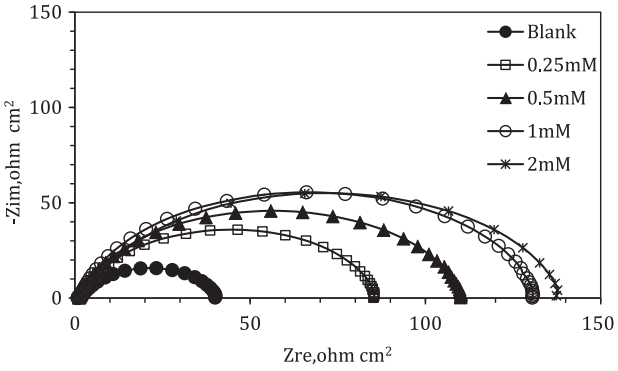

Fig. 6. Nyquist plots for mild steel in 1 M HCl at 30 °C in the absence and presence of various concentrations of PTD.

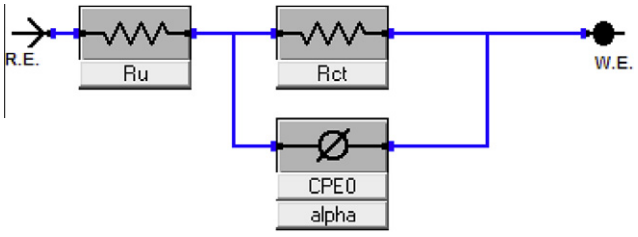

Fig. 7. Equivalent circuit model used to fit the impedance data for mild steel.

increases with an increase in the PT derivatives' concentrations, the inhibition efficiency increases. The inhibition efficiency (P_{EIS}%) was calculated according to Eq. (2):

$$P_{EIS} = \left(1 - \frac{R_{ct}^0}{R_{ct}}\right) \times 100 \quad (2)$$

In this equation, R_{ct} and R_{ct}^0 are the charge transfer resistance with and without the PT derivatives, respectively. The EIS results showed that the inhibition efficiencies increase in the order of PTD < PT < PTO. It can be deduced from the EIS results that PTO is the best among the studied inhibitors. The calculated double-layer capacitance values, C_{dl}, derived from the CPE parameters according to Eq. (3) are listed in Table 2 [33]:

$$C_{dl} = \left(A\, R_{ct}^{1-n}\right)^{1/n} \quad (3)$$

In general, the values of the double-layer capacitance, C_{dl}, decreased in the presence of inhibitors. The decrease in C_{dl} is likely due to a decrease in the local dielectric constant and/or an increase

Please cite this article in press as: A.Y. Musa et al., Molecular dynamic and quantum chemical calculations for phthalazine derivatives as corrosion inhibitors of mild steel in 1 M HCl, Corros. Sci. (2011), doi:10.1016/j.corsci.2011.12.005

Table 2
Fitted impedance parameters of mild steel in 1 M HCl in the absence and the presence of different concentrations of PT derivatives at 30 °C.

	C_{inh} (mM)	R_{ct} (ohm cm^2)	R_u (mohm cm^2)	CPE_0 (μS × s^a/cm^2)	α	C_{dl} (μF cm^2)	τ (ms)	P_{EIS} (%)
	0	42	1.056	774	0.78	294.0	12.30	0.00
PT	0.25	105.3	0.6092	452.7	0.77	181.3	19.1	60
	0.5	137.9	0.7204	402.3	0.76	161.3	22.2	70
	1	154.3	0.8289	204.3	0.81	92.3	14.2	73
	2	207.9	0.6617	277.2	0.76	112.9	23.5	80
PTO	0.25	111.8	4.717	153.4	0.89	93.2	10.4	62
	0.5	165.3	0.5151	164.8	0.87	96	15.9	75
	1	204.5	0.5642	133.1	0.88	82.6	16.9	80
	2	230.5	0.5199	303.7	0.76	128.7	29.7	82
PTD	0.25	87.38	0.8499	299	0.83	145.1	12.7	52
	0.5	111.3	1.09	229.2	0.85	122.17	13.6	62
	1	131.8	1.211	176.3	0.87	101.84	13.4	68
	2	143.7	0.6254	322	0.78	136.77	19.7	70

in the thickness of a protective layer at the electrode surface, which would therefore enhance the corrosion resistance of the studied mild steel in a 1 M HCl solution at 30 °C.

The relaxation time (τ) of a surface state is the time required for the return of the charge distribution to equilibrium after an electrical disturbance. In the case when no distributed element is inserted to replace the double-layer capacitance, it is defined [33] as:

$$\tau = C_{dl}R_{ct} \quad (4)$$

In general, upon increasing the concentration of the inhibitors, the time of the adsorption process becomes much higher, which corresponds to a slow adsorption process [33]. The obtained τ values in the absence and presence of PT, PTO and PTD at 2 mM are 12.3, 23.5 and 19.7 ms, respectively. In this investigation, the additions of PT derivatives caused an increase in τ values in general. PTO has the highest value of τ, implying that PTO was the slowest in the adsorption processes.

4.2. Potentiodynamic polarization (PDP) measurements

Polarization (cathodic and anodic) curves for mild steel in 1 M HCl at 30 °C in both the absence and presence of various concentrations of PT, PTO and PTD derivatives are shown in Figs. 8–10, respectively. Electrochemical kinetic parameters for PT, PTO and PTD, including the Tafel constants for the cathodic (β_C) and anodic (β_A) reactions, the corrosion current densities (i_{corr}) and the corrosion potential (E_{corr}), were obtained and are listed in Table 3. The inhibition efficiency (P_{PDP}%) was calculated according to Eq. (5) and is depicted in Table 3

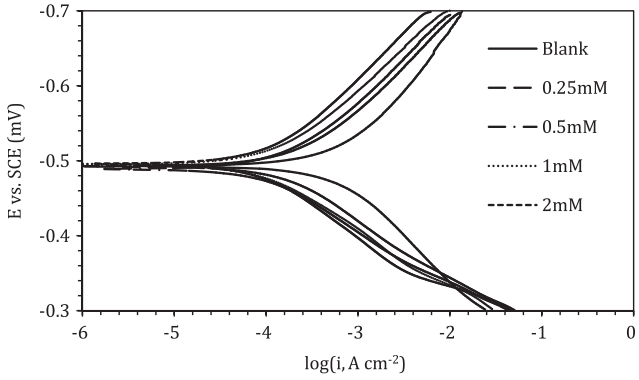

Fig. 8. Potentiodynamic polarization curves for mild steel in 1 M HCl at 30 °C in the absence and presence of various concentrations of PT.

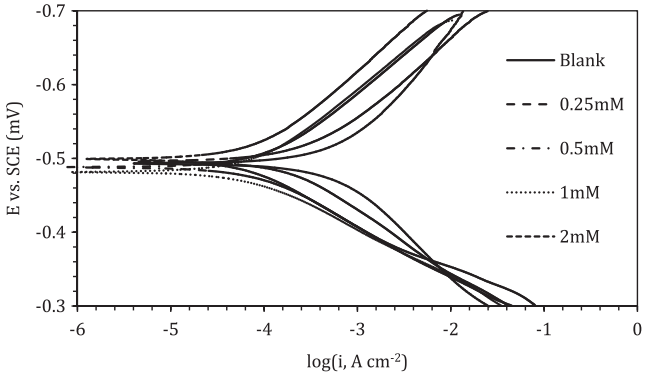

Fig. 9. Potentiodynamic polarization curves for mild steel in 1 M HCl at 30 °C in the absence and presence of various concentrations of PTO.

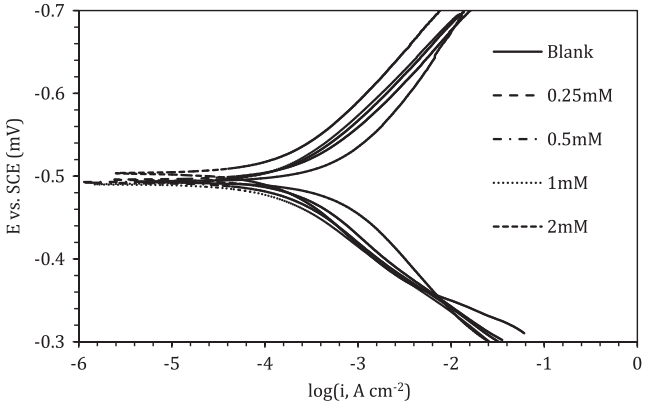

Fig. 10. Potentiodynamic polarization curves for mild steel in 1 M HCl at 30 °C in the absence and presence of various concentrations of PTD.

$$P_{PDP} = \left(1 - \frac{i_{corr(inh)}}{i_{corr(uninh)}}\right) \times 100 \quad (5)$$

In this equation, $i_{corr(uninh)}$ and $i_{corr(inh)}$ are the corrosion current densities in the absence and presence of the inhibitor, respectively. The results for all inhibitors indicated that the i_{corr} decreases proportionally with an increase in inhibitor concentration, and thus, it leads to an increase in P_{PDP}%. Based on the minimum inhibitor efficiency, the PT derivatives are ranked as follows: PTD < PT < PTO. It was observed that the presence of the inhibitors minimize the i_{corr}. The lowest value of 61.1 μA cm^{-2} was obtained with PTO, indicating that PTO is the most effective corrosion inhibitor among the

Please cite this article in press as: A.Y. Musa et al., Molecular dynamic and quantum chemical calculations for phthalazine derivatives as corrosion inhibitors of mild steel in 1 M HCl, Corros. Sci. (2011), doi:10.1016/j.corsci.2011.12.005

Table 3
Polarization parameters of mild steel in 1 M HCl in absence and presence of different concentration of PT derivatives at 30 °C.

	C_{inh} (mM)	β_A (V/decade)	β_c (V/decade)	I_{corr} (μA/cm^2)	$-E_{corr}$ (mV$_{vs.\ SCE}$)	P_{PDP} (%)
	0	0.12	0.14	660.1	491	0
PT	0.25	0.09	0.11	171	493	74
	0.5	0.08	0.10	115	489	83
	1	0.08	0.10	104	495	84
	2	0.09	0.11	95.3	496	86
PTO	0.25	0.07	0.10	102	479	85
	0.5	0.07	0.10	91.3	488	86
	1	0.07	0.10	74.8	482	89
	2	0.07	0.10	61.1	499	91
PTD	0.25	0.10	0.11	245	496	63
	0.5	0.09	0.11	182	492	72
	1	0.09	0.11	155	490	77
	2	0.09	0.11	148	503	78

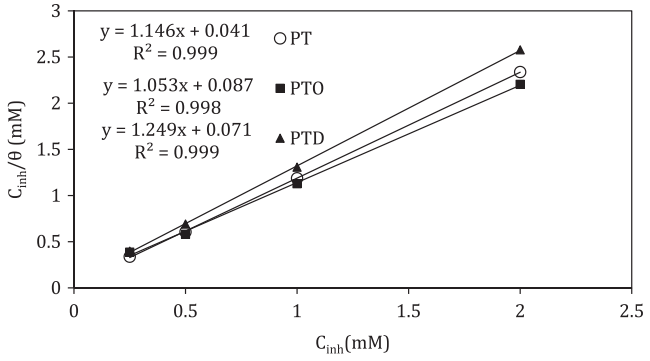

Fig. 11. Adsorption isotherms of PT, PTO and PTO molecules on the mild steel surface in 1 M HCl at 30 °C.

Table 4
Adsorption parameter of PT derivatives for mild steel in 1 M HCl at 30 °C.

	PT	PTO	PTD
K_{ads}	24037.33	11481.89	13958.54
ΔG^0_{ads} (kJ/mol)	−35.55	−33.68	−34.18

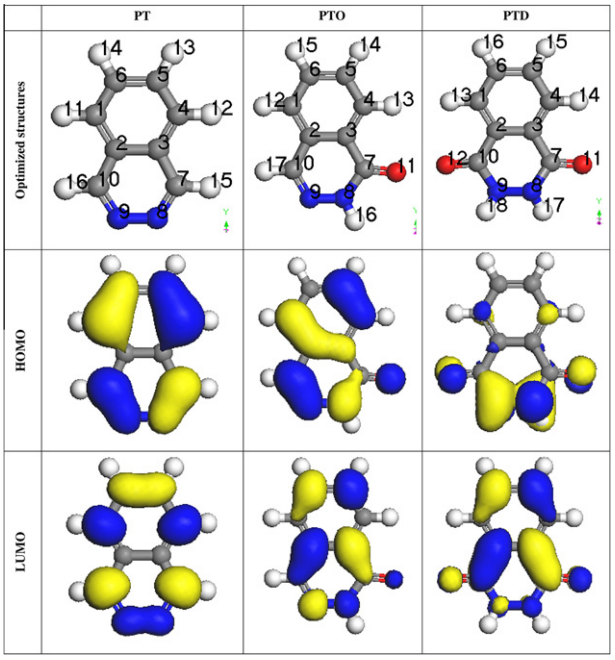

Fig. 12. Optimized structures and molecular orbital plots for PT derivatives using AM1.

derivatives studied. The results of the potentiodynamic polarization confirm the EIS results showing that PTO is a better inhibitor than PT and PTD.

In acidic solutions, the anodic process of corrosion is the passage of metal ions from the metal surface into the solution. The principal cathodic process is the discharge of hydrogen ions to produce hydrogen gas or the reduction of oxygen. The inhibitor may affect either one or both of the anodic and cathodic processes [34], and in these experiments, the anodic Tafel slope β_a and cathodic Tafel slope β_C of the PT derivatives were found to change with inhibitor concentration. In addition, when the change in the E_{corr} value is greater than 85 mV, a compound can be recognized as an anodic- or a cathodic-type inhibitor [36,37]. The largest displacement of the corrosion potential (E_{corr}) in our experiments was approximately 12 mV (Table 3) for all inhibitors studied. The changes in these three values indicate that the inhibitors affected both of these reactions [35].

Further inspection of Figs. 8–10 shows that the presence of these inhibitors slightly shifts the corrosion potential (E_{corr}) towards the cathode. It is also worth noting that the value of β_a changes dramatically with the addition of PT derivatives, much more so than the value of β_C. This indicates that the PT derivatives behave anodically more than cathodically, and thus, the PT derivatives are probably adsorbed on the anodic part of the mild steel surface. Based on the above discussion, it can be deduced that with an increase of inhibitor concentration, the dissolution of mild steel is inhibited, and its P_{PDP}% increases. These results indicated that the increase in inhibitor efficiency with concentration might be attributed to the formation of a barrier film that provides protection against the acid medium. This barrier film on the metal surface would be caused by the adsorption of these compounds onto the mild steel surface through interactions involving the π-electrons of the heterocyclic structure of the inhibitors and the vacant *d-orbitals* of the iron surface atoms [38].

4.3. Adsorption isotherm

Because the corrosion of metals is associated with a negative change in the Gibbs free energy, an absorption isotherm must be calculated for the system in order to obtain the adsorption free energy $\left(\Delta G^0_{ads}\right)$ values; this isotherm is very necessary for understanding the mechanism of corrosion inhibition. In order to do this, the adsorption behavior must be known. It was assumed that the adsorption of these inhibitors followed the Langmuir adsorption isotherm. The Langmuir adsorption isotherm, presented in Eq. (6), is most often used to calculate the equilibrium

Table 5
Quantum chemical parameters derived for PT derivatives calculated with the AM1,PM3 and MNDO methods.

AM1	E_{HOMO} (eV)	E_{LUMO} (eV)	$\Delta E = (E_{HOMO}-E_{LUMO})$ (eV)	$I = -E_{HOMO}$ (eV)	$A = -E_{LUMO}$ (eV)	χ	η	ΔN
PT	−9.553	−0.903	8.650	9.553	0.903	5.228	4.325	0.205
PTO	−9.255	−0.636	8.619	9.255	0.636	4.946	4.310	0.238
PTD	−9.785	−1.013	8.772	9.785	1.013	5.399	4.386	0.183
PM3								
PT	−9.659	−1.017	8.642	9.659	1.017	5.338	8.642	0.096
PTO	−9.137	−0.845	8.292	9.137	0.845	4.991	8.292	0.121
PTD	−9.685	−1.112	8.573	9.685	1.112	5.398	8.573	0.093
MDNO								
PT	−9.430	−0.922	8.508	9.430	0.922	5.176	4.254	0.214
PTO	−9.214	−0.802	8.412	9.214	0.802	5.008	4.206	0.237
PTD	−10.012	−1.124	8.887	10.012	1.124	5.568	4.444	0.161

Table 6
Calculated Mulliken atomic charges for the three PT derivatives using AM1.

	Atom No.	Type	Charge	Atom No.	Type	Charge
PT	1	C	−0.065	2	C	−0.078
	3	C	−0.078	4	C	−0.065
	5	C	−0.084	6	C	−0.084
	7	C	0.003	8	N	−0.132
	9	N	−0.132	10	C	0.003
PTO	1	C	−0.080	2	C	−0.035
	3	C	−0.122	4	C	−0.025
	5	C	−0.108	6	C	−0.067
	7	C	0.458	8	N	−0.408
	9	N	−0.069	10	C	−0.045
	11	O	−0.383			
PTD	1	C	−0.040	2	C	−0.086
	3	C	−0.086	4	C	−0.040
	5	C	−0.085	6	C	−0.085
	7	C	0.419	8	N	−0.310
	9	N	−0.310	10	C	0.419
	11	O	−0.355	12	O	−0.355

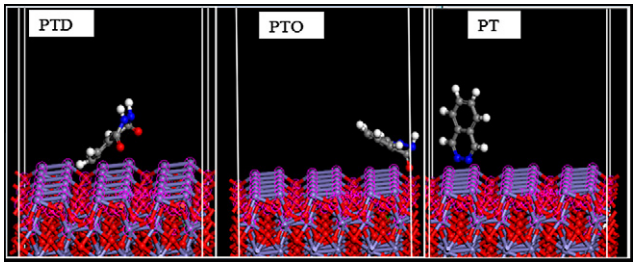

Fig. 13. Mode of adsorption of the PT derivatives on the Fe_2O_3 (1 1 0) surface.

constant (K_{ads}). The value θ in Eq. (6) represents the degree of surface coverage obtained from the potentiodynamic data [39]. Fig. 11 shows C_{inh}/θ vs. C_{inh} and the straight line obtained for PT, PTO and PTD. The values of ΔG^0_{ads} are obtained using Eq. (8). The values of the intercept are used to calculate K_{ads}. Table 4 shows the calculated values of K_{ads} and ΔG^0_{ads}

$$\frac{C_{inh}}{\theta} = \frac{1}{K_{ads}} + C_{inh} \quad (6)$$

$$\theta = \frac{P_{PDP}}{100} \quad (7)$$

$$\Delta G^0_{ads} = -RT\ln(55.5K_{ads}) \quad (8)$$

In general, for values of ΔG^0_{ads} up to −20 kJ mol^{-1}, the adsorption types were regarded as physisorption, where the inhibition occurs due to the electrostatic interactions between the charged molecules and the charged metal. For ΔG^0_{ads} values of −40 kJ mol^{-1} or smaller were regarded as chemisorption, which is due to the charge sharing or a transfer from the inhibitor molecules to the metal surface to form a covalent bond. Table 4 showed that the calculated values of were in the range of −33.7 to 35.8 kJ mol^{-1}. This suggested that the PT derivatives were adsorbed chemically onto the mild steel surface [40,41].

4.4. Quantum chemical calculations and molecular dynamics simulations

The frontier molecular orbital density distributions of three PT derivatives are presented, as calculated by AM1, in Fig. 12. The reactive abilities of the studied inhibitors are considered to be closely related to their frontier molecular orbitals, including the highest occupied molecular orbital (HOMO) and the lowest unoccupied molecular orbital (LUMO). A higher HOMO energy (E_{HOMO}) of the molecule correlates to a higher electron-donating ability to an appropriate acceptor molecule with a low-energy empty molecular orbital [36,32]. Thus, high values of E_{HOMO} facilitate adsorption, and the inhibition efficiency is enhanced. Similar relations were found between the inhibition efficiency and the energy gap (ΔE) in the frontier molecular orbitals ($\Delta E = E_{LUMO}-E_{HOMO}$). The LUMO energy ($E_{LUMO}$) indicates the ability of the molecule to accept electrons; the lower the value of E_{LUMO}, the more probable it is that the molecule will accept electrons. Lower values of the energy difference, ΔE, will cause a good inhibition efficiency, as the energy to remove an electron from the highest-energy occupied molecular orbital will be low [42].

As shown in Fig. 12, the HOMO in these molecules is focused mainly around the nitrogen and oxygen atoms. In addition, the HOMO is focused around the aromatic system for PT and PTO more than it is for PTD. The values of E_{LUMO} and E_{HOMO} that were calculated using AM1, PM3 and MNDO are listed in Table 5. The high inhibition efficiency of PTO can be attributed to the high value of the E_{HOMO} and E_{LUMO} and the low values of ΔE. Moreover, it has been proved that local electron densities or charges are important in many chemical reactions and in the physicochemical properties of compounds. Mulliken atomic charge distributions for the PT derivatives are depicted in Table 6. In these data, it can be seen that all N, O and most C atoms carry negative charges. This indicates that these atoms are the negative charge centers that could offer electrons to the iron atoms on the metal surface to form a coordinate bond [43,44]. Therefore, the PT derivatives were likely adsorbed onto the anodic part of the mild steel surface, decreasing the dissolution of the metal. This behavior was confirmed by potentiodynamic measurements, where the change in β_a is more pronounced than that in β_C. Table 6 also reveals that the electron charge density on the N9 atom increased proportionally with the inhibition ability of the PT derivatives (PTD < PT < PTO). This indicates that N9 is the bonding center of the studied inhibitors.

In addition, there are certain quantum-chemical parameters that can be related to metal–inhibitor interactions and the validi-

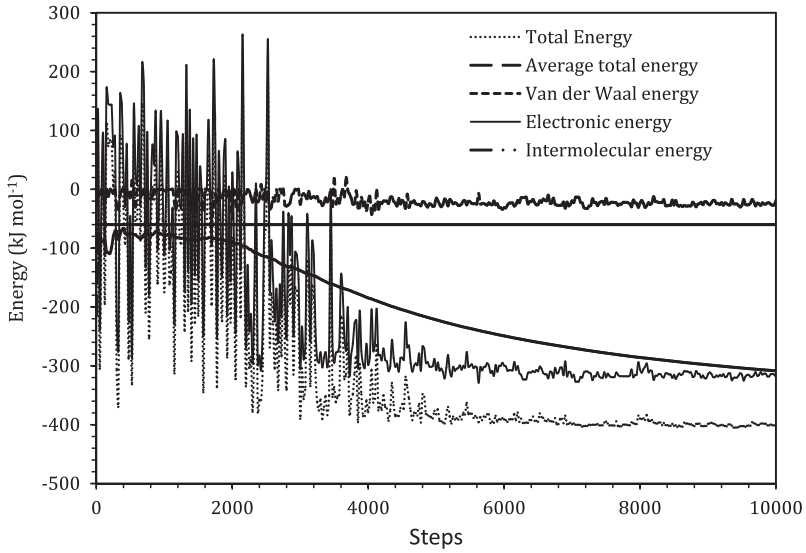

Fig. 14. Total energy distribution for the PTO/Fe_2O_3 system during the energy optimization process.

Table 7
Outputs and descriptors calculated by the Monte Carlo simulation for adsorption of PT derivatives on Fe_2O_3 (110).

	Total energy (kJ/mol)	Adsorption energy (kJ/mol)	Rigid adsorption energy (kJ/mol)	Deformation energy (kJ/mol)	dE_{ad}/dN_i
PT	−83.05	−559.61	−597.18	37.57	−133.75
PTO	−685.92	−625.96	−785.4	159.49	−149.61
PTD	−379.36	−458.85	−846.67	387.81	−109.67

ties of which are generally accepted [42]. The obtained values of ionization potential (I) and electron affinity (A) were considered for the calculation of the electronegativity (χ) and global hardness (η). The fraction of electrons transferred from the inhibitor molecules to the metallic atom (ΔN) was calculated according to Pearson [45], as shown in Eq. (9)

$$N = \frac{\chi_{Fe} - \chi_{inh}}{2(\eta_{Fe} + \eta_{inh})} \tag{9}$$

where a theoretical value for the electronegativity of bulk iron was used, $\chi_{Fe} = 7$ eV, and a global hardness of $\eta_{Fe} = 0$ was used [42]. These quantities are related to A and I

$$\chi = \frac{(I + A)}{2(10)} \tag{10}$$

$$\eta = \frac{(1 - A)}{2} \tag{11}$$

From Table 5, it is possible to observe that PTO has a lower value of global hardness among the studied inhibitors. The fraction of transferred electrons for this molecule is also the largest that we observed for these derivatives, followed by PT and then PTD [42].

Monte Carlo and molecular dynamics simulations were performed on a system with the PT derivative molecules and a Fe_2O_3 surface, as shown in Fig. 13. The Fe_2O_3 surface layer was selected for the simulation based on the fact that the iron metal already oxidized before introducing the acid solution. The total energy, average total energy, Van der Waals energy, electrostatic energy and intermolecular energy for the PTO/Fe_2O_3 surface are presented in Fig. 14. Monte Carlo docking was performed on each of the 100 conformations, and each of the docked structures was energetically relaxed. The outputs and descriptors calculated by the Monte Carlo simulation, including the total adsorption, rigid adsorption and deformation energies, are presented in Table 7. The total energy is defined as the sum of the energies of the adsorbate components. The adsorption energy is defined as the sum of the rigid adsorption energy and the deformation energy for the adsorbate components. The rigid adsorption energy, deformation energy and adsorption energy concern the energy released (or required) when the relaxed adsorbate components (PT derivatives) are adsorbed on the metal. The rigid adsorption energy is the energy released (or required) when the unrelaxed adsorbate components (i.e., before the geometry optimization step) are adsorbed on the metal. The deformation energy is the energy released when the adsorbed adsorbate components are relaxed on the metal surface. Table 7 shows (dE_{ads}/dN_i), which is the energy of metal-adsorbate configurations where one of the adsorbate components has been removed [46,47].

As is clear in Table 7, the adsorption energies of the studied molecules increased in the order of PTD < PT < PTO, and PTO gave the maximum negative adsorption energy. Therefore, PTO exhibited greater inhibition abilities as compared to the PT and PTD molecules [48,49]. These findings confirmed the results that were obtained from the EIS and potentiodynamic measurements.

5. Conclusions

(1) Corrosion inhibition was achieved using PT derivatives as corrosion inhibitors for mild steel in 1 M HCl at 30 °C. The highest inhibition efficiency was exhibited by PTO, with a value of 90%.
(2) The results obtained from the EIS and PDP showed that the corrosion inhibition efficiencies increased with an increase in inhibitor concentration.
(3) Potentiodynamic polarization measurements showed that the PT derivatives act as mixed inhibitor types but that they are more pronounced on the anodic component.
(4) The adsorptions of PT derivatives followed the Langmuir adsorption isotherm, and the adsorption mechanisms of inhibitors on mild steel surface from 1 M HCl occurred chemically.
(5) Quantum chemical parameters were calculated using semi-empirical equations (AM1, MNDO and PM3).
(6) The adsorption behavior of PT derivatives was simulated using Monte Carlo molecular dynamics.

Please cite this article in press as: A.Y. Musa et al., Molecular dynamic and quantum chemical calculations for phthalazine derivatives as corrosion inhibitors of mild steel in 1 M HCl, Corros. Sci. (2011), doi:10.1016/j.corsci.2011.12.005

(7) Experimental results showed that the inhibition efficacies increased in the order PTD < PT < PTO. This result was also confirmed by Monte Carlo simulations, where the adsorption energies increased in the order PTD < PT < PTO. Therefore, PTO is the most effective inhibitor among the studied inhibitors.

Acknowledgments

The authors gratefully acknowledge the Universiti Kebangsaan Malaysia for the financial support of this project under Grant Number UKM-GUP-2011-035.

References

[1] R.W. Revie, H.H. Uhlig, Corrosion and Corrosion Control an Introduction to Corrosion Science and Engineering, Wiley, New Jersey, 2008.
[2] N.O. Eddy, B.I. Ita, Q.S. AR, DFT and quantum chemical studies on the inhibition potentials of some carbozones for the corrosion of mild steel in HCl, J. Mol. Model 17 (2011) 359–376.
[3] S. Xia, M. Qiua, L. Yua, F. Liua, H. Zhao, Molecular dynamics and density functional theory study on relationship between structure of imidazoline derivatives and inhibition performance, Corros. Sci. 50 (2008) 2021–2029.
[4] A.K. Singha, M.A. Quraishi, The effect of some bis-thiadiazole derivatives on the corrosion of mild steel in hydrochloric acid, Corros. Sci. 52 (2010) 1373–1385.
[5] Y. Tang, Y. Chen, W. Yang, Y. Liu, X. Yin, J. Wang, Electrochemical and theoretical studies of thienyl-substituted amino triazoles on corrosion inhibition of copper in 0.5 M H_2SO_4, J. Appl. Electrochem. 38 (2008) 1553–1559.
[6] Y. Yan, W. Li, L. Cai, B. Hou, Electrochemical and quantum chemical study of purines as corrosion inhibitors for mild steel in 1 M HCl solution, Electrochim. Acta 53 (2008) 5953–5960.
[7] S.G. Zhang, W. Lei, M.Z. Xia, F.Y. Wang, QSAR study on N-containing corrosion inhibitors: quantum chemical approach assisted by topological index, J. Mol. Struct. (Theochem) 732 (2005) 173–182.
[8] G. Bereket, E. Hür, C.Ö. Retir, Quantum chemical studies on some imidazole derivatives as corrosion inhibitors for iron in acidic medium, J. Mol. Struct. (Theochem) 578 (2002) 79–88.
[9] G. Gece, S. Bilgic, Quantum chemical study of some cyclic nitrogen compounds as corrosion inhibitors of steel in NaCl media, Corros. Sci. 51 (2009) 1876–1878.
[10] S.L. Li, Y.G. Wang, S.H. Chen, R. Yu, S.B. Lei, H.Y. Ma, De X. Liu, Some aspects of quantum chemical calculations for the study of Schiff base corrosion inhibitors on copper in NaCl solutions, Corros. Sci. 41 (1999) 1769–1782.
[11] A.Y. Musa, A.H. Kadhum, A.B. Mohamad, M.S. Takriff, Experimental, theoretical study on the inhibition performance of triazole compounds for mild steel corrosion, Corros. Sci. 52 (2010) 3331–3340.
[12] Z. Yang, Y. Zhao, Adsorption of His-tagged peptide to Ni, Cu and Au (100) surfaces: molecular dynamics simulation, Eng. Anal. Bound. Elem. 31 (2007) 402–409.
[13] J. Bartley, N. Huynh, S.E. Bottle, H. Flitt, T. Notoya, D.P. Schweinsberg, Computer simulation of the corrosion inhibition of copper in acidic solution by alkyl esters of 5-carboxybenzotriazole, Corros. Sci. 45 (2003) 81–96.
[14] Z. Xu, S. Yuan, H. Yan, C. Liu, Adsorption of histidine, histidine-containing peptides on Au(111): a molecular dynamics study, Colloids and Surfaces A: Physicochem. Eng. Aspects 380 (2011) 135–142.
[15] Y. Tang, L. Yao, C. Kong, W. Yang, Y. Chen, Molecular dynamics simulations of dodecylamine adsorption on iron surfaces in aqueous solution, Corros. Sci. 53 (2011) 2046–2049.
[16] T.T. Qin, J. Li, H.Q. Luo, M. Li, N.B. Li, Corrosion inhibition of copper by 2, 5-dimercapto-1, 3, 4-thiadiazole monolayer in acidic solution, Corros. Sci. 53 (2011) 1072–1078.
[17] J. Zeng, J. Zhang, X. Gong, Molecular dynamics simulation of interaction between benzotriazoles and cuprous oxide crystal, Comp. Theo. Chem. 963 (2011) 110–114.
[18] J. Zhang, G. Qiao, S. Hu, Y. Yan, Z. Ren, L. Yu, Theoretical evaluation of corrosion inhibition performance of imidazoline compounds with different hydrophilic groups, Corros. Sci. 53 (2011) 147–152.
[19] M.K. Awad, M.R. Mustafa, M.M. Abo Elnga, Computational simulation of the molecular structure of some triazoles as inhibitors for the corrosion of metal surface, J. Mol. Struct. (Theochem) 959 (2010) 66–74.
[20] L.X. Yu, MA.H. Yi, M. Shuai1, Z. Min, Self-assembled monolayers of stearic imidazoline on copper electrodes detected using electrochemical measurements, XPS, molecular simulation and FTIR, Chinese Sci. Bull. 54 (2009) 374–381.
[21] K.F. Khaled, Studies of iron corrosion inhibition using chemical, electrochemical and computer simulation techniques, Electrochim. Act 55 (2010) 6523–6532.
[22] E.E. Oguzie, C.K. Enenebeaku, C.O. Akalezi, S.C. Okoro, A.A. Ayuk, E.N. Ejike, Adsorption and corrosion-inhibiting effect of Dacryodis edulis extract on low-carbon-steel corrosion in acidic media, J. Colloid. Interf. Sci. 349 (2010) 283–292.
[23] A.Y. Musa, A.H. Kadhum, M.S. Takriff, A.R. Daud, S.K. Kamarudin, Evaluation of Ethylenediaminetetra-acetic acid di-sodium salt as corrosion inhibitor for mild steel in 1 m hydrochloric acid, Basic Appl. Sci. 2 (2008) 956–960.
[24] ASTM G1-3, Standard Practice for Preparing, Cleaning, and Evaluating Corrosion Test Specimens, 2003.
[25] A.Y. Musa, A.H. Kadhum, A.B. Mohamad, A.R. Daud, M.S. Takriff, S.K. Kamarudin, A comparative study of the corrosion inhibition of mild steel in sulphuric acid by 4, 4-dimethyloxazolidine-2-thione, Corros. Sci. 51 (2009) 2393–2399.
[26] A.Y. Mus, A.A.H. Kadhum, A.B. Mohamad, M.S. Takriff, A.R. Daud, S.K. Kamarudin, Adsorption isotherm mechanism of amino organic compounds as mild steel corrosion inhibitors by electrochemical measurement method, J. Cent. South Univ. Technol. 17 (2010) 34–39.
[27] M. Benabdellaha, A. Tounsib, K.F. Khaledc, B. Hammouti, Thermodynamic, chemical and electrochemical investigations of 2-mercapto benzimidazole as corrosion inhibitor for mild steel in hydrochloric acid solutions, Arab. J. Chem. 4 (2011) 17–24.
[28] K.F. Khaled, Molecular modeling and electrochemical investigations of the corrosion inhibition of nickel using some thiosemicarbazone derivatives, J. Appl. Electrochem. doi:10.1007/s10800-010-0252-1.
[29] E.H. El Ashrya, A. Nemr, S.A. Esawyb, S. Ragab, Corrosion inhibitors: Part II: quantum chemical studies on the corrosion inhibitions of steel in acidic medium by some triazole, oxadiazole and thiadiazole derivatives, Electrochim. Acta 51 (2006) 3957–3968.
[30] H. Jua, Z. Kaic, Yan Li, Aminic nitrogen-bearing polydentate Schiff base compounds as corrosion inhibitors for iron in acidic media: a quantum chemical calculation, Corros. Sci. 50 (2000) 865–871.
[31] B. Prathaba, V. Subramanianb, T.M. Aminabhavi, Molecular dynamics simulations to investigate polymer–polymer and polymer–metal oxide interactions, Polymer 48 (2007) 409–416.
[32] K.F. Khaled, Monte Carlo simulations of corrosion inhibition of mild steel in 0.5 M sulphuric acid by some green corrosion inhibitors, J. Solid State Electr. 13 (2009) 1743–1756.
[33] F. Bentiss, C. Jamaba, B. Mernari, H. El-Attari, L. El Kadi, M. Lebrini, M. Traisnel, M. Lagrenée, Corrosion control of mild steel using 3,5-bis(4-methoxyphenyl)-4-amino-1,2,4-triazole in normal hydrochloric acid medium, Corros. Sci. 51 (2008) 1628–1635.
[34] V.R. Saliyana, A.V. Adhikari, Quinolin-5-ylmethylene-3-{[8-(trifluoromethyl)quinolin-4-yl]thio}propanohydrazide as an effective inhibitor of mild steel corrosion in HCl solution, Corros. Sci. 50 (2008) 55–61.
[35] A.Y. Musa, A.H. Kadhum, A.B. Mohamad, M.S. Takriff, A.R. Daud, S.K. Kamarudin, Inhibition of aluminum alloy 2024 corrosion by 4-amino-5-phenyl-4H-1, 2, 4-trizole-3-thiol in highly sulfuric acid solution, Adv. Mater. Res. 93 (2010) 354–357.
[36] K.F. Khaled, M.A. Amin, N.A. Al-Mobarak, On the corrosion inhibition, adsorption behaviour of some benzotriazole derivatives during copper corrosion in nitric acid solutions: a combined experimental and theoretical study, J. Appl. Electrochem. 40 (2010) 601–613.
[37] F. Xu, J. Duan, S. Zhanga, B. Hou, The inhibition of mild steel corrosion in 1 M hydrochloric acid solutions by triazole derivative, Mater. Lett. 62 (2008) 4072–4074.
[38] K.F. Khaled, Mohammed A. Amin, Computational and electrochemical investigation for corrosion inhibition of nickel in molar nitric acid by piperidines, J. Appl. Electrochem. 38 (2008) 1609–1621.
[39] F. Xu, B. Hou, Triazole derivatives as corrosion inhibitors for mild steel in hydrochloric acid solution, Acta Metall. Sin. 22 (2009) 247–254.
[40] S. Zhang, Z. Tao, W. Li, B. Hou, Some new triazole derivatives as inhibitors for mild steel corrosion in acidic medium, J. Appl. Electrochem. 38 (2008) 289–295.
[41] W. Li, Q. He, C. Pei, B. Hou, Experimental, theoretical investigation of the adsorption behaviour of new triazole derivatives as inhibitors for mild steel corrosion in acid media, Electrochim. Acta 52 (2007) 6386–6394.
[42] T. Arslana, F. Kandemirli, E.E. Ebenso, I. Lovec, H. Alemu, Quantum chemical studies on the corrosion inhibition of some sulphonamides on mild steel in acidic medium, Corros. Sci. 51 (2009) 35–47.
[43] M. Özcan, İ. Dehri, Electrochemical and quantum chemical studies of some sulphur-containing organic compounds as inhibitors for the acid corrosion of mild steel, Prog. Org. Coat. 51 (2004) 181–187.
[44] M.A. Amin, K.F. Khaledb, S.A. Fadl-Allah, Testing validity of the Tafel extrapolation method for monitoring corrosion of cold rolled steel in HCl solutions – Experimental, theoretical studies, Corros. Sci. 55 (2010) 140–151.
[45] I.B. Obot, N.O. Obi-Egbedi, Theoretical study of benzimidazole, its derivatives, their potential activity as corrosion inhibitors, Corros. Sci. 52 (2010) 657–660.
[46] K.F. Khaled, Corrosion control of copper in nitric acid solutions using some amino acids – a combined experimental, theoretical study, Corros. Sci. 52 (2010) 3225–3234.
[47] K.F. Khaled, Experimental, atomistic simulation studies of corrosion inhibition of copper by a new benzotriazole derivative in acid medium, Electrochim. Acta 54 (2009) 4345–4352.
[48] K.F. Khaled, Experimental and molecular dynamics study on the inhibition performance of some nitrogen containing compounds for iron corrosion, Mater. Chem. Phys. 124 (2010) 760–767.
[49] K.F. Khaled, Electrochemical behavior of nickel in nitric acid and its corrosion inhibition using some thiosemicarbazone derivatives, Electrochim. Acta 55 (2010) 5375–5383.

Please cite this article in press as: A.Y. Musa et al., Molecular dynamic and quantum chemical calculations for phthalazine derivatives as corrosion inhibitors of mild steel in 1 M HCl, Corros. Sci. (2011), doi:10.1016/j.corsci.2011.12.005